Shahrood University of Technology
Iranian Society of Mining Engineering (IRSME)
Journal of Mining and Environment (JME)
journal homepage: www.jme.shahroodut.ac.ir
THOMSON REUTERS

# On Propagation Mechanism of Cracks Emanating from Two Neighboring Holes in Cubic Concrete Specimens under Various Lateral Confinements

Mohammad Davood Yavari[1], Hadi Haeri[2*], Vahab Sarfarazi[3] and Mohammad Fatehi Marji[4], Hossain Ali Lazemi[1]

*1- Department of mining Engineering, Bafgh Branch, Islamic Azad University, Bafgh, Iran*
*2- State Key Laboratory for Deep GeoMechanics and Underground Engineering, Beijing, China*
*3- Department of Mining Engineering, Hamedan University of Technology, Hamedan, Iran*
*4- Mine Exploitation Engineering Department, Faculty of Mining and Metallurgy, Institution of Engineering, Yazd University, Yazd, Iran*

***Article Info***

*Received 12 May 2021*
*Received in Revised form 29 July 2021*
*Accepted 6 August 2021*
*Published online 6 August 2021*

*DOI:10.22044/jme.2021.10834.2054*

***Keywords***

*Experimental modeling*
*Crack propagation path*
*Confining stress*
*Pre-holed specimens*
*PFC2D*

***Abstract***

The propagation mechanism of cracks emanating from two holes within the concrete specimens is studied by considering the effects of different lateral compressive stresses. The experimental part of this research work is carried out on some specially prepared pre-cracked specimens with two neighbouring holes under only a uniaxial compression in the laboratory. The numerical modeling part is performed under both the uniaxial compresion and the lateral confinment by the 2D particle flow code (PFC2D). It is shown that the lateral confinement may change the path of crack propagation in a specimen compared to that of the uniaxially-loaded one. Various senarios of the mixed mode radial crack propagation around the holes are obtained, and both the wing (induced tensile) cracks and secondary (shear) cracks are produced and propagated in various paths due to a change in the confining pressure. The fracturing pattern changes from a single tensile crack to that of the several shear bands by increasing the confining pressure. Also the number of shear cracks is increased by increasing the lateral confinement. On the other hand, as the confining pressure increases, the wing cracks start their growth from the walls and reach the center of the cracks under high confinements.

## 1. Introduction

Understanding the failure mechanism of rock structures containing micro- and macro-cracks under various loading conditions is of most importance to the geomechanics who are concerned with the design of rock structures related to various engineering fields such as the geological, mining, civil, petroleum, energy, and environmental engineering. The geomaterials such as rocks and concretes are among the mostly used structural materials, and contain the main skeleton of many engineering projects such as buildings, dams, tunnels, underground openings, and mines. Therefore, the failure mechanism, crack propagation, and crack coalescence of these brittle materials have been investigated by many researchers [1-7].

The failure mechanism of rocks and concrete structures under compressive loading have been investigated in the recent years [8-12]. Most of the investigations have considered the material samples with pre-existing cracks, and have found that the crack extension in brittle materials is due to the propagation of wing cracks in the direction of the applied compressive load [13-15]. They have clarified that in most of the experimental tests and numerical investigations, the tensile and shear cracks initiate from the tips of the cracks already existing in the rock and concrete specimens under various loading conditions [13].

It has been observed that these induced cracks mainly initiate from the crack tips, and continue their propagation toward the boundaries in the direction of the maximum principal stress or they may coalesce with one another [14]. In the case of brittle materials such as rocks and concretes, due to their relatively low tensile strength, the formation of

*Corresponding author: h.haeri@bafgh-iau.ac.ir (H. Haeri).*

wing (tensile) cracks is more dominant than those of the secondary (shear) cracks. The wing cracks may propagate in curve paths so that the secondary cracks can originate from them. Therefore, the two co-planar and oblique cracks can be produced [17, 18]. The failure and fracture mechanisms due to the process of crack propagation in brittle rocks and rock-like materials (concretes) have been studied in the recent decades by Particle Flow Code (PFC) [19-31]. These research work results were in line with the experimental results, which indicated that PFC was able to simulate the progressive failure of the brittle rock. Hazzard et al. [32] have used a two-dimensional (2D) simulation procedure to study the failure process in rocks. They clarified that the simulated failure process of the hardest rocks such as granite was very close to that of the laboratory test. These 2D investigations may not be able to properly simulate all rock features affecting the rock behaviors under compression. The discrete element method has been used by Park et al. [33] for comparing the rock failure process results for small-scale and large-scale discontinuity sets by using the two-dimensional particle flow code (PFC2D) and the universal distinct element code (UDEC), respectively. They concluded that the density of rock joints affected the post-peak failure of rocks, and changed the rock behavior from brittle to ductile as the number of discontinuity increased in the rock mass. Although these models demonstrate the effects of discontinuities on the failure behavior of rocks, they may not be able to exactly simulate the actual rock masses. Holt et al. [34] have studied the effects of cement content of rock-like glass on the elastic modulus and strength of the material sample using the calibrated results of the PFC2D simulated models with the experimental laboratory results. Yoon [35] has combined the experimental design and optimization procedures in order to establish a suitable statistical approach for simulating a geo-material sample in PFC2D. This advance method is used to calibrate the particle assemblies by the well-optimized micro-parameters based on the laboratory testing results. In this procedure, the uniaxial peak strength and elastic moduli of various rocks were optimized for the contact-bonded particle assemblies of the geo-material samples. Most of these studies did not emphasize on the post-failure behavior of geomaterials. The mechanical behavior of the synthetic soft rocks has been numerically simulated by Cho et al. [36] using a calibrated PFC2D based on the arbitrary rigid particles of sphere/disc shape. The numerically achieved rock stiffness, uniaxial strength, and its envelope were reasonably fitted with their corresponding laboratory results. However, the real rock behavior includes non-linearity at small load levels in the pre-failure zone of the stress-strain curves and also in the post-failure zone. The numerically modelled samples usually cannot model the non-linearity in rock behavior before and after the peak strength of the actual stress-strain curves. Hao [27] has accomplished some numerical and experimental investigations on the pre-cracked rock specimens in order to study the process of crack propagation under compression. They found that the numerical results were in good agreement with the corresponding experimental ones. Some experiments have also been carried out on the rock-like specimens by Zhang [26] in order to study the crack propagation mechanism of closed and open pre-existing cracks.

Some experiments were conducted by Zhao [30]. The deformation behavior and strength of the sandstone specimens have been investigated by Yang [15]. The photographic monitoring technic was used to study the behavior of the sandstone specimens by considering the effect of crack inclination angles. They investigated the crack propagation and crack coalescence phenomena due to co-planar cracks. Li [31] has used three different types of brittle materials in order to investigate the mechanism of failure and crack extension in the specimens. He conducted some uniaxial compression tests on these specimens (each containing either one or two pre-existing cracks), and observed the crack extension paths for various scenarios. In the previous works, the influence of confining pressure on the sample containing hole and notch has not been analyzed. In this work, the laboratory tests and the numerical simulations of some specially prepared cubic specimens of concrete are accomplished in order to investigate the failure mechanism and fracturing process in brittle materials. These specimens contain two neighboring holes and two cracks placed on the above and below these holes (as shown in Figure 1). The effect of lateral stress on the fracturing mechanism of the specimen is studied. The numerical simulation of these specimens under lateral confinement is accomplished in the PFC2D software, which is a 2D particle flow code. Comparing the corresponding experimental and numerical results show the accuracy of the results, and also approves the validity and flexibility of the numerical modelling.

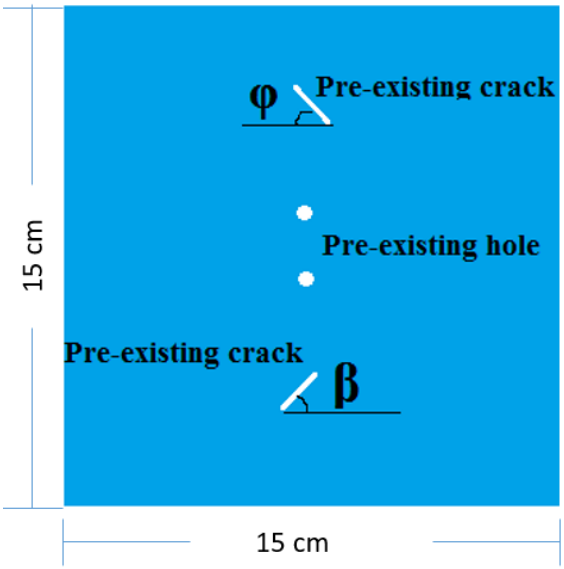


**Figure 1. A schematic configuration (in 2D) of the specially designed concrete specimens.**

## 2. Experimentally observed crack propagation process in concrete specimens

In this section, the specially prepared cubic specimens containing holes and cracks were tested in the laboratory in order to visualize the simultaneous effects of cracks and holes on the failure mechanism of the concrete.

### 2.1. Preparing appropriate cubic concrete specimens

The rectangular concrete models with two holes and two cracks are to be provided for an experimental test. Therefore, the cubic specimens with 150 mm in length, height, and thickness were provided, as shown in Figure 1. Table 1 gives the mechanical properties and specifications of the concrete specimens prepared in the laboratory.

Six pre-cracked cubic concrete specimens with two holes were constructed, as shown in Figures 2(a) to 2(f).

**Table 1 shows the specifications of the concrete specimens including the physical/mechanical properties and specifications.**

| Sample types | Sample mixture | Material ratio | Density (kg/m$^3$) | Wave velocity (m/s) | UCS (MPa) | Tensile strength (MPa) |
|---|---|---|---|---|---|---|
| I | Cement/grain/water | 1/0.5/1 | 3000 | 3500 | 28.3 | 2.9 |

### 2.2. Crack growth process for cubic specimens of concrete containing cracks and two holes

The fracturing mechanism of the pre-cracked cubic specimens of the concrete with two cracks just above and below the two neighboring holes was experimentally evaluated under compression. The path of the propagated wing cracks originated from the pre-existing cracks towards the holes and boundaries of the specimen for six different scenarios are given in Figures 3(a) to 3(e). The laboratory tests were accomplished on the cubic specimens of the concrete with cracks and holes. These specimens were specially prepared for six scenarios: (a) $\varphi = 30^\circ$, $\beta = 30^\circ$, (b) $\varphi = 45^\circ$, $\beta = 45^\circ$, (c) $\varphi = 55^\circ$, $\beta = 55^\circ$, (d) $\varphi = 55^\circ$, $\beta = 0^\circ$, (e) $\varphi = 55^\circ$, $\beta = 90^\circ$, and (f) $\varphi = 90^\circ$, $\beta = 90^\circ$). The breaking stresses for these tests were obtained, and the propagation path of the pre-existing cracks was observed. In most of these tests, it was observed that the cracks started their propagation from the tips of the pre-existing cracks toward the holes and toward the specimens' boundaries in the direction of maximum principal stress. In some cases, the radial cracks may also start their propagation from the boundaries of the holes (Figure 3). The surface of tensile cracks was smooth without a pulverized material. However, shear cracks had a wavy surface with a pulverized material.

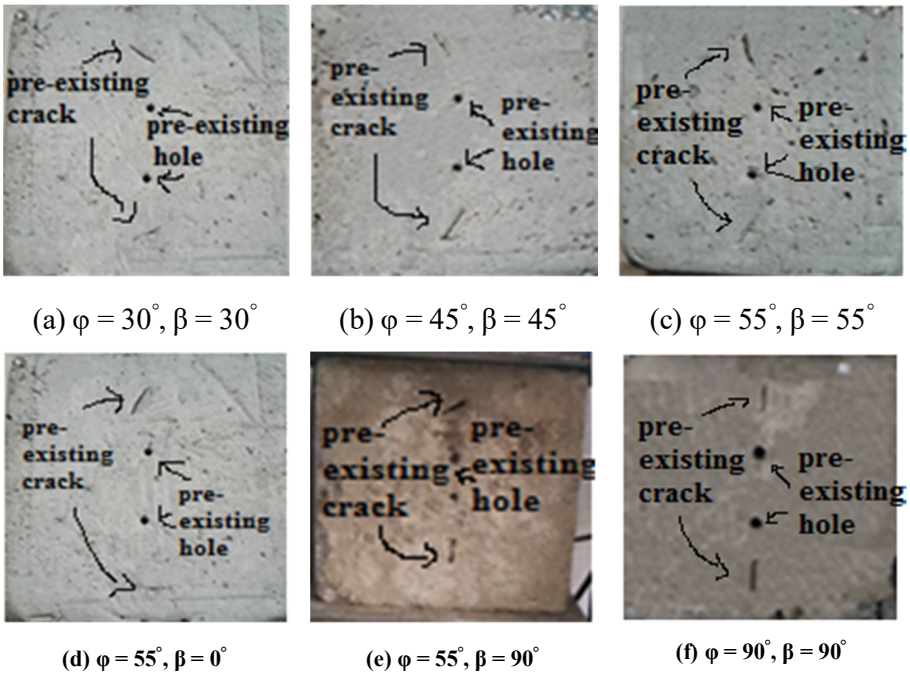


(a) φ = 30°, β = 30° (b) φ = 45°, β = 45° (c) φ = 55°, β = 55°

(d) φ = 55°, β = 0° (e) φ = 55°, β = 90° (f) φ = 90°, β = 90°

**Figure2. Cubic concrete specimens with cracks and two holes used for the experimental tests.**

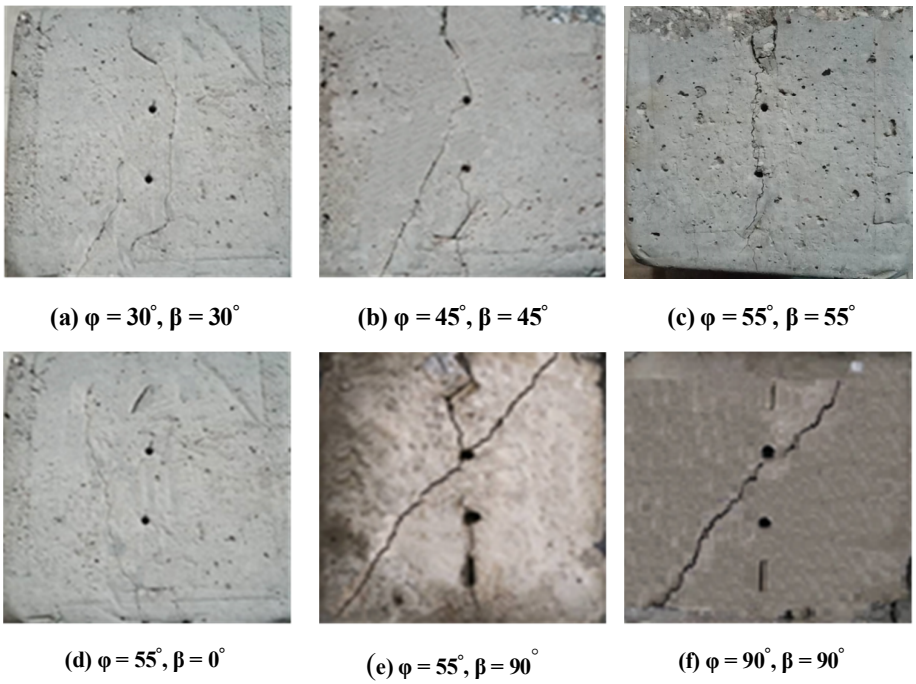

**(a) φ = 30°, β = 30° (b) φ = 45°, β = 45° (c) φ = 55°, β = 55°**

**(d) φ = 55°, β = 0° (e) φ = 55°, β = 90° (f) φ = 90°, β = 90°**

**Figure 3. Crack growth paths of the pre-cracked cubic concrete specimens with two holes obtained from the experimental tests for different crack locations and arrangements, i.e. for the six cases of (a) φ = 30°, β = 30°, (b) φ = 45°, β = 45°, (c) φ = 55°, β = 55°, (d) φ = 55°, β = 0°, (e) φ = 55°, β = 90°, and (f) φ = 90°, β = 90°.**

## 3. Model calibration procedure for cubic specimens

The versatile uniaxial compressive strength test was used as a standard test for calibrating the numerical models of the cubic specimens in PFC2D. In this calibration procedure, the standard uniaxial compressive strength tests for geo-materials were assumed, and the modelled specimens were considered as an assembly of

particles through the following four main steps: i) the particle assembly was generated and packed, ii) the isotropic condition of stress distribution within the assembly was established, iii) the floating particles in the assembly were eliminated to obtain a robust simulated model, iv) the particle bonds were installed for all the particles within the assembly. The plane strain condition was used in the software. The tensile crack was initiated when the applied load exceeded from the normal strength of bonds, while the shear crack was initiated when the applied load exceeded from the shear strength of bonds.

Potyondy and Cundall (2004) have used a standard calibration procedure for the discrete element modeling of the geo-material samples. In this research work, the cubic samples of concrete were modelled by adopting the same procedure. Therefore, the particle assembly of the geo-material (concrete specimen) was generated using a total number of 5,615 particles. During the test, the two lateral walls of the assembly were moved toward each other at a standard speed of 0.016 m/s. The micro-properties for the calibrated particle assembly are given in Table 2.

**Table 2. Micro-properties used to represent the intact cubic concrete specimen in the modelled sample.**

| Parameter | Value | Parameter | Value |
|---|---|---|---|
| Type of particle | disc | Parallel bond radius multiplier | 1 |
| Density (kg/m$^3$) | 3000 | Young modulus of parallel bond (GPa) | 40 |
| Minimum radius (mm) | 0.27 | Parallel bond stiffness ratio | 1.7 |
| Size ratio | 1.56 | Particle friction coefficient | 0.4 |
| Porosity ratio | 0.08 | Parallel bond normal strength, mean (MPa) | 30 |
| Damping coefficient | 0.7 | Parallel bond normal strength, SD (MPa) | 2 |
| Contact young modulus (GPa) | 40 | Parallel bond shear strength, mean (MPa) | 30 |
| Stiffness ratio | 1.7 | Parallel bond shear strength, SD (MPa) | 2 |

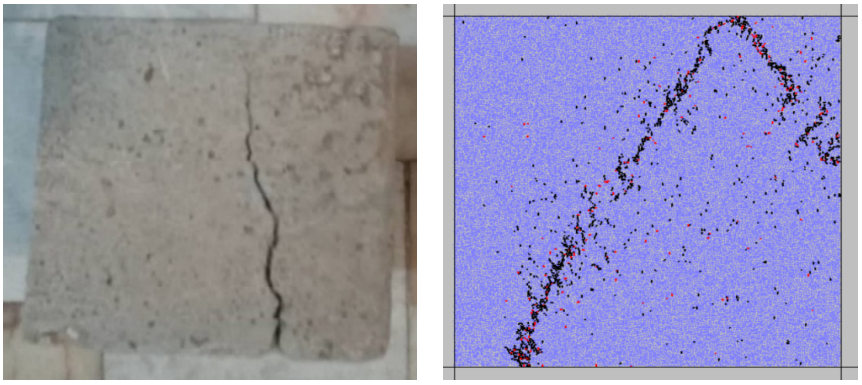

(a) (b)

**Figure 4. failure pattern in a) physical sample, b) PFC2D model.**

Figures 4a and 4b show the uniaxial compressive strength test carried out in the laboratory and modelled by PFC2D, respectively. It was observed that the numerical and laboratory tests were well-matching with each other.

However, the numerical and experimental values for the uniaxial compressive strengths of the modeled and tested samples are presented in Table 3. As it can be seen, these two values are very close to each other. In both cases, one major fracture develops within the model.

**Table 3. Uniaxial compressive strengths of physical and numerical samples.**

| | |
|---|---|
| Experimental compressive strength (MPa) | 28.3 |
| Numerical compressive strength (MPa) | 28.1 |

The numerical results for the uniaxial compression test are shown in Figure 5. In this figure, the red lines correspond to the shear cracks, and the black lines represent the tensile cracks developed during the test. It was shown that the tensile cracks were more dominant than the shear cracks in this model test, which was close to the results already obtained experimentally in the previous section.

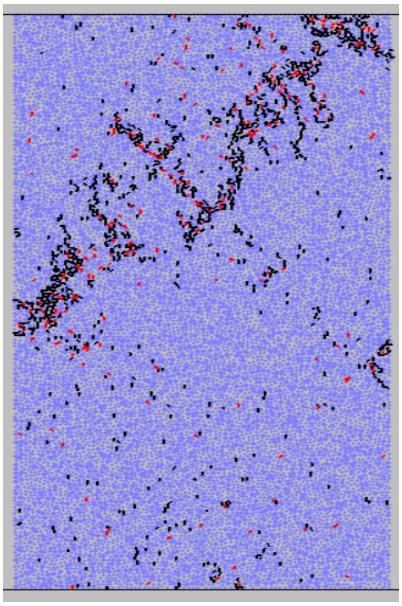

**Figure 5. Tensile cracks (black lines) and shear cracks (red lines) observed in the numerical compression test of the intact cubic concrete specimen.**

## 4. Numerical simulation of pre-cracked cubic concrete specimen containing two holes

The pre-cracked cubic concrete specimens were numerically simulated by PFC2D, and the experimentally crack propagation paths observed in the laboratory tests were verified in this section.

The modeled rectangular concrete specimens are shown in Figure 6. The various positions of cracks with respect to the two holes are shown in these figures. The modelled samples were uniaxially loaded, and then the lateral confinement was incrementally added to investigate its effects on the failure strength and fracture patterns considering various orientations of the two cracks related to the two holes.

### 4.1. Modeling specimens with particle flow code

The discrete element method (DEM) developed by Cundall (1979) for modelling the 2D geomaterial specimens known as the particle flow code (PFC2D) was used in order to model the cubic concrete specimens containing two cracks just above and below two vertically placed holes at their central parts. Howevere, in the modified PFC2D, as proposed by Potyondy and Cundall 2004, the geomaterial specimen is represented by an assembly of rigid particles. The particles are bonded together at their contact points by the contact forces, and can move independently within the assembly.The 2D DEM code using a central finite difference scheme was used to calculate the contact forces and the movements of the particles in the assembly under a specified applied load. The linear and non-linear contact mdels considering the possible frictional sliding between the particles could be used in the form of linear contact models and parallel bond models. The relations between the contact forces and relative movements of the particles was considered to be elastic within the assembly. The linear contact model was used in this work, which provided liear elastic stress-strain relations for the modelled sample. The calibrated micro-properties used for generating a parallel bond model in PFC2D for the cubic concrete specimens include i) a contact modulus between the balls (circles), ii) the stiffness ration $k_n/k_s$, iii) the friction coefficient, iv) the normal and shear strengths of the parallel bonds, v) the parallel bond radius and its multiplier, vi) the parallel bond modulus and stiffness ratio, and vii) the standard deviation for the ratio of normal and shear bond strengths to those of the mean strengths. The calbration procedure could be conducted to predict the appropriate micro-properties for the models based on the actual values of the material strengths gained from the laboratory tests on the cubic specimens of concrete. The trail-and-error approach was used as a versatile calibration procedure in PFC2D, which related the micro-mechanical properties of the models with the macro-properties obtained through the actual laboratory tests.

Based on the micro-mechanical parameters given in Table 4, two types of cubic concrete specimens were calibrated in the form of two particle assemblies. The calibrated models for the cubic concret specimens were of the size 150 × 150 × 150 mm, and the assembly contained 6421 particles. In this modeling procedure, the low standard speed of 0.016 m/s was adapted to move the two lateral walls of the modelled specimen toward each other and assure the integrity and robustness of this geomaterial particle assembly.

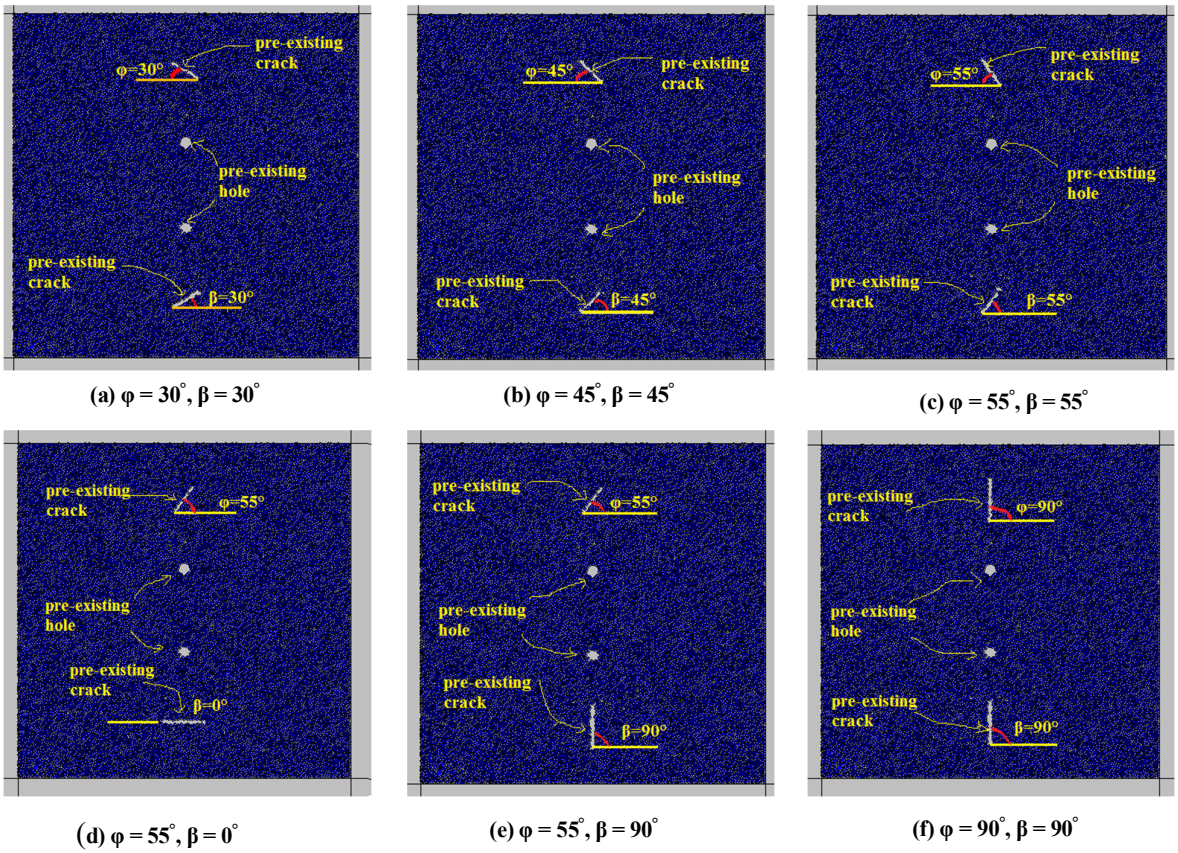


**Figure 6. Rectangular sections of the modelled cubic concrete specimens. Various specifications are given in parts (a) to (e).**

**Table 4. Micro-properties used to represent the modelled cubic concrete specimens.**

| Parameter | Value | Parameter | Value |
|---|---|---|---|
| Type of particle | disc | Stiffness ratio | 3 |
| density | 3000 | Particle friction coefficient | 0.5 |
| Minimum radius | 0.27 | contact bond normal strength, mean (MPa) | 24 |
| Size ratio | 1.56 | contact bond normal strength, SD (MPa) | 2 |
| Porosity ratio | 0.08 | contact bond shear strength, mean (MPa) | 24 |
| Damping coefficient | 0.7 | contact bond shear strength, SD (MPa) | 2 |
| Contact young modulus (GPa) | 8 | | |

The compressive strength of the numerically modeled specimens was compared with those experimentally measured in the laboratory, and tabulated in Table 5. Comparing these mechanical properties show that they are well-matching, and therefore, validate the correctly calibrated numerical values for the modelled particle assemblies of different specimens.

In this work, the physical problems and experimental tests were carried out in three dimensions, while the numerical simulations were established in two dimensions. The crack analyses of the cubic concrete specimens were mainly in two dimensions, and the tensile mode (Mode I) and the shear mode (Mode II) of the fracture propagation mechanism were considered in this work.

In this analysis, the mechanism of crack propagation and coalescence in the pre-cracked cubic specimens of concrete, considering the strength of the bridge areas, were investigated. These specimens contained two vertical neighboring holes containing two cracks just above and below the holes. Figures 7a to 7e show the numerical modeling of the crack propagation paths for the simulated cubic concrete specimens. The six different types of specimens were numerically modeled, and the results obtained were graphically shown in the Figure 7. These figures show six scenarios of the fracturing patterns for the cubic

concrete specimens, which are comparable to those already obtained experimentally through the laboratory tests (shown in Figures 3a to 3e). In the numerical simulation of the crack analyses of the pre-cracked cubic specimens with two vertical holes, two cracks with different arrangements and locations were considered, and the specimens were under a uniaxial compression. Similar to the experimental study of the six scenarios, (a) $\varphi = 30^{\circ}$, $\beta = 30^{\circ}$, (b) $\varphi = 45^{\circ}$, $\beta = 45^{\circ}$, (c) $\varphi = 55^{\circ}$, $\beta = 55^{\circ}$, (d) $\varphi = 55^{\circ}$, $\beta = 0^{\circ}$, (e) $\varphi = 55^{\circ}$, $\beta = 90^{\circ}$, and (f) $\varphi = 90^{\circ}$, $\beta = 90^{\circ}$ were modelled. Checking the numerical results in Figures 7a to 7e with the corresponding experimental results given in Figures 3a to 3e, respectively, show that the comparison is meaningful. In most cases, the cracks start their propagation from the crack tips. A major diagonal fracture was developed in these models.

**Table 5. Failure strengths of various cubic concrete specimens used in this work.**

| Numerical failure stress in MPa | Experimental failure stress in MPa | Various types of cubic concrete specimtens |
|---|---|---|
| 28.1 | 28.3 | Intact (without crack) |
| 22.2 | 21.2 | (a) $\varphi = 30^{\circ}$, $\beta = 30^{\circ}$ |
| 14.8 | 14.1 | (b) $\varphi = 45^{\circ}$, $\beta = 45^{\circ}$ |
| 12 | 11.1 | (c) $\varphi = 55^{\circ}$, $\beta = 55^{\circ}$ |
| 12.5 | 11.5 | (d) $\varphi = 55^{\circ}$, $\beta = 0^{\circ}$ |
| 10 | 11.1 | (e) $\varphi = 55^{\circ}$, $\beta = 90^{\circ}$ |
| 23 | 22.4 | (f) $\varphi = 90^{\circ}$, $\beta = 90^{\circ}$ |

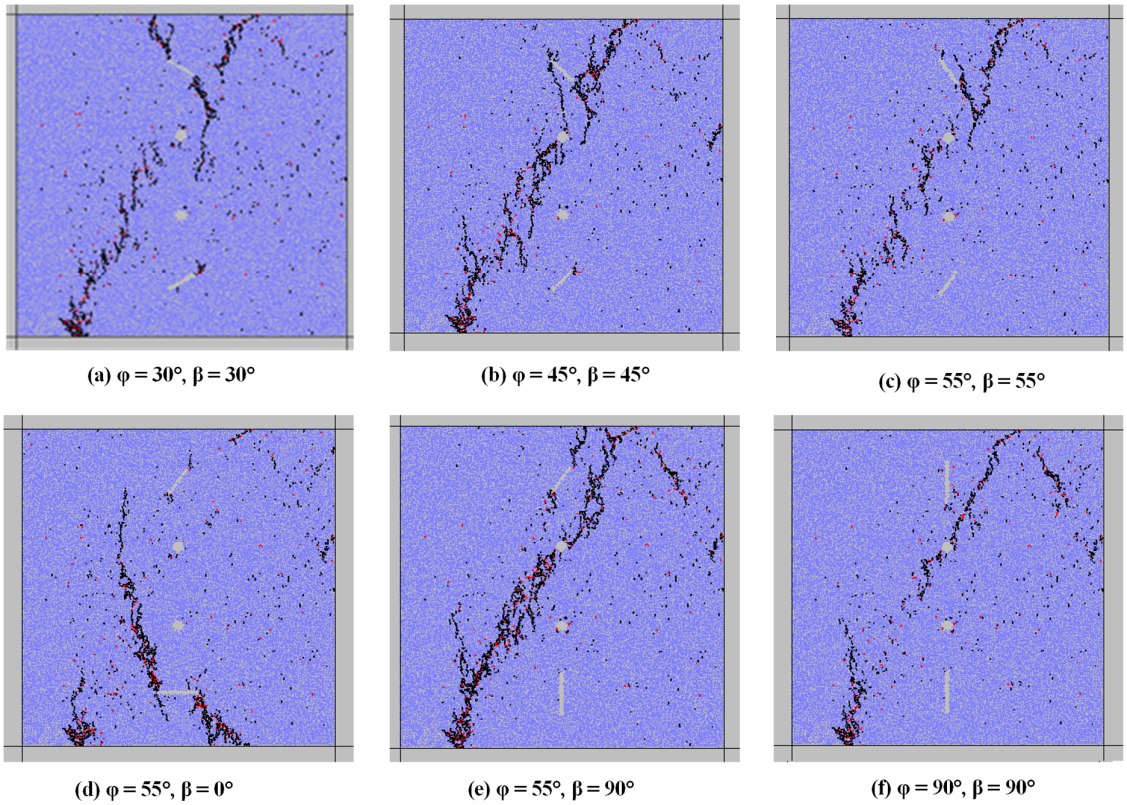


**Figure 7. Results of numerical modeling for the pre-cracked cubic concrete specimens with two holes just above and below the holes. The specimens tested under uniaxial compression and six different arrangements and locations of the two cracks were considered: (a) $\varphi = 30^{\circ}$, $\beta = 30^{\circ}$, (b) $\varphi = 45^{\circ}$, $\beta = 45^{\circ}$, (c) $\varphi = 55^{\circ}$, $\beta = 55^{\circ}$, (d) $\varphi = 55^{\circ}$, $\beta = 0^{\circ}$, (e) $\varphi = 55^{\circ}$, $\beta = 90^{\circ}$, and (f) $\varphi = 90^{\circ}$, $\beta = 90^{\circ}$.**

### 4.2. Effects of confining pressure on crack propagation patterns of modeled specimens

In this section, the effects of lateral confinements on the fracturing mechanism of the specially modelled cubic concrete specimens with two holes and two cracks were investigated. The lateral confinements used for this modeling were 1 MPa, 3 MPa, 6 MPa, and 9 MPa.

The effects of confining pressure on the fracturing paths of the two cracks in the cubic concrete specimens with two vertically located holes are given in Figures 8 to 11, considering the changes in the confining pressure as 1 MPa, 3 MPa, 6 MPa, and 9 MPa, respectively. The wing cracks generated from the tips of the pre-existing cracks of the modelled specimens under low confinements are shown in Figs. 9 and 10. On the other hand, as the confining pressure increases, the wing cracks start their growth from the walls and reach the center of the cracks under high confinements, as shown in Figs. 11 and 12, respectively. The high confining pressure suppresses the tensile crack growth pattern and increases the shear crack growth mechanism of the specimens. It means that the failure mechanism of the specimen changes from a single diagonally fractured pattern to that of the several cross-sectional fractured sets as the confining pressure is increased. However, the fracture length is decreased by increasing the lateral confinement. When the confining pressure is low, one crack may start its propagation, while for the case of high confinement, the failure process is controlled by the two cracks.

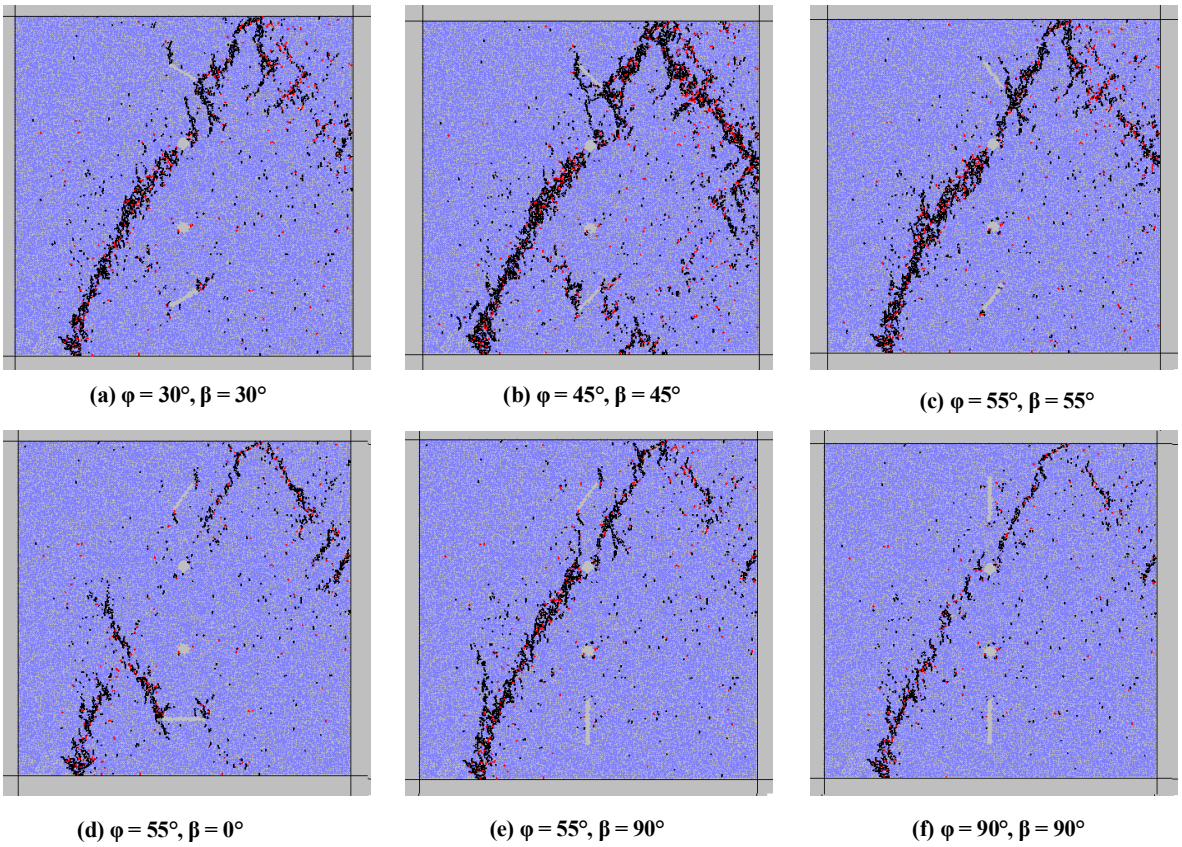

**(a) φ = 30°, β = 30°** **(b) φ = 45°, β = 45°** **(c) φ = 55°, β = 55°**

**(d) φ = 55°, β = 0°** **(e) φ = 55°, β = 90°** **(f) φ = 90°, β = 90°**

**Figure 8. Effect of low confining pressure (1 MPa) on the mechanism of crack growth in the numerically modeled cubic specimens considering different pre-existing crack arrangements as (a) φ = 30°, β = 30°, (b) φ = 45°, β = 45°, (c) φ = 55°, β = 55°, (d) φ = 55°, β = 0°, (e) φ = 55°, β = 90° , (f) φ = 90°, β = 90°.**

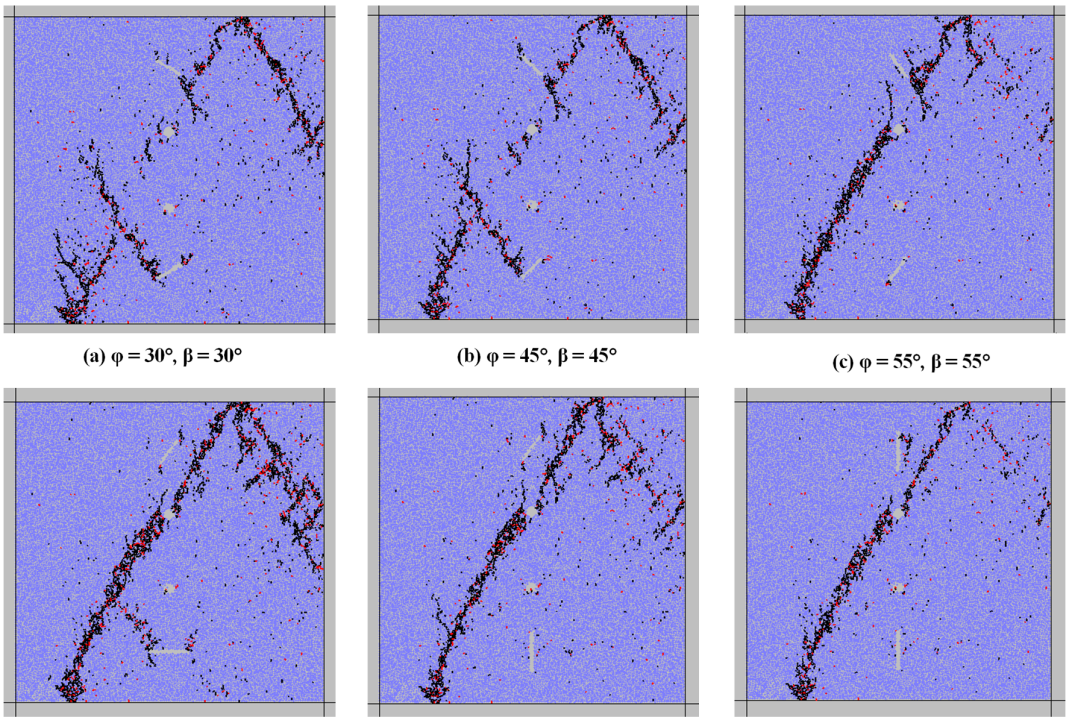


**Figure 9. Effect of low to medium confining pressure (3 MPa) on the mechanism of crack growth in the numerically modeled cubic specimens considering different pre-existing crack arrangements as (a) φ = 30°, β = 30°, (b) φ = 45°, β = 45°, (c) φ = 55°, β = 55°, (d) φ = 55°, β = 0°, (e) φ = 55°, β = 90°, (f) φ = 90°, β = 90°.**

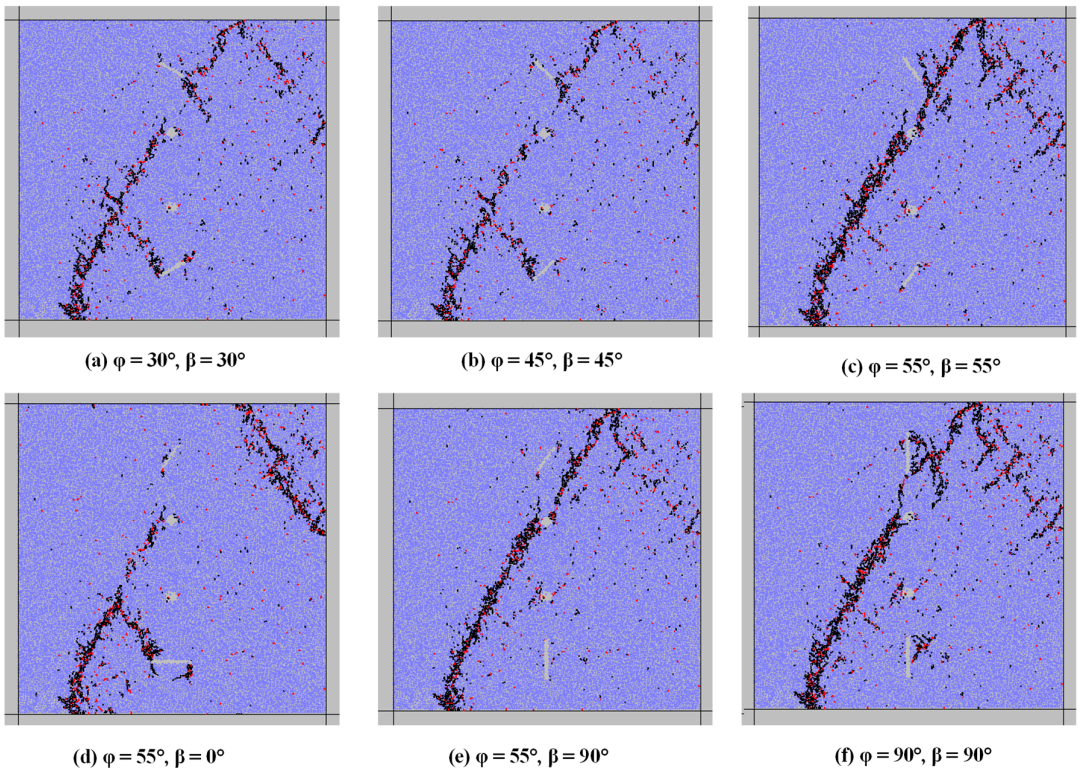


**Figure 10. Effect of relatively high confining pressure (6 MPa) on the mechanism of crack growth in the numerically modeled cubic specimens considering different pre-existing crack arrangements as (a) φ = 30°, β = 30°, (b) φ = 45°, β = 45°, (c) φ = 55°, β = 55°, (d) φ = 55°, β = 0°, (v) φ = 55°, β = 90°, (f) φ = 90°, β = 90°.**

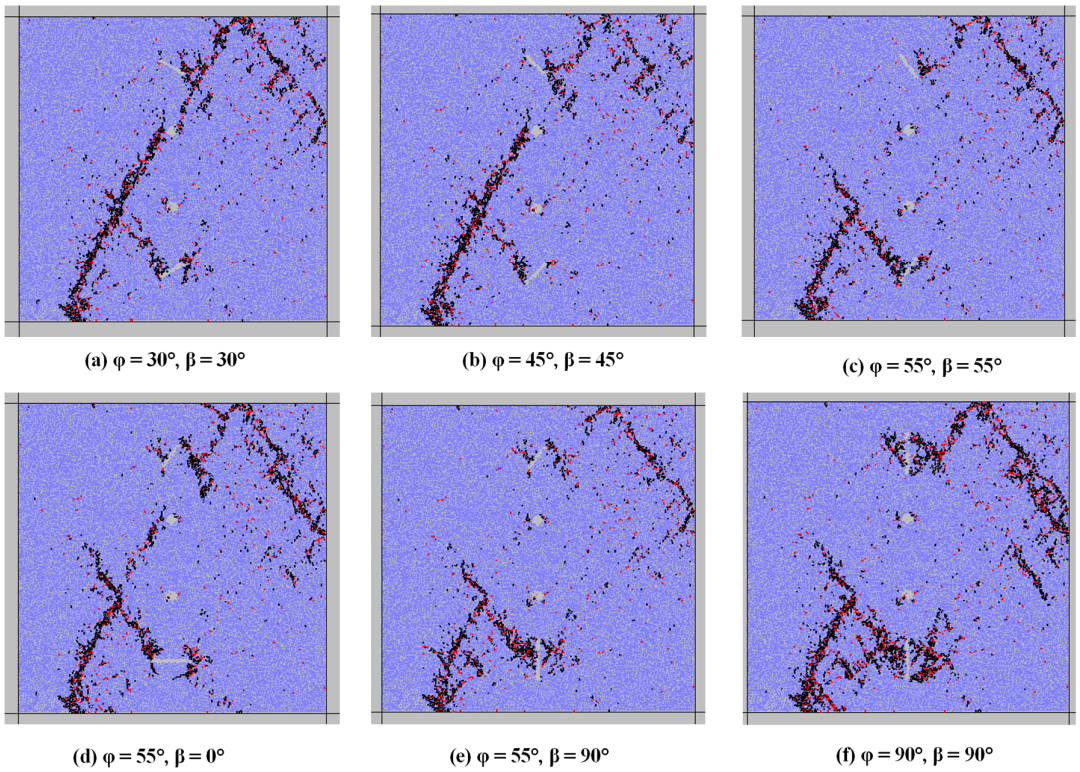


**Figure 11. Effect of high confining pressure (9 MPa) on the mechanism of crack growth in the numerically modeled cubic specimens considering different pre-existing crack arrangements as (a) φ = 30°, β = 30°, (b) φ = 45°, β = 45°, (c) φ = 55°, β = 55°, (d) φ = 55°, β = 0°, (e) φ = 55°, β = 90°, (f) φ = 90°, β = 90°.**

From the above findings, it could be concluded that in a fixed confining pressure, the number of cracks were increased by increasing the notch angle. Also the fracturing pattern changed from a single tensile crack to that of the several shear bands by increasing the confining pressure.

### 4.3. Pre-cracked cubic specimens under uniaxial compression

The compressive strength of the pre-cracked cubic specimen of concrete was somewhat lower than that of the intact (un-cracked) one. In this section, the ratio of the final failure stress ($\sigma_F$) to the strength ($\sigma_F/\sigma_c$) of the pre-cracked specimens containing two holes and two cracks was obtained. The average unconfined compressive strength (i.e. $\sigma_c$) of the intact specimens was 28.1 MPa.

Based on the configurations shown in Figure 3, six different scenarios were considered, i.e. (a) $\varphi = 30^\circ$, $\beta = 30^\circ$, (b) $\varphi = 45^\circ$, $\beta = 45^\circ$, (c) $\varphi = 55^\circ$, $\beta = 55^\circ$, (d) $\varphi = 55^\circ$, $\beta = 0^\circ$, (e) $\varphi = 55^\circ$, $\beta = 90^\circ$, and (f) $\varphi = 90^\circ$, $\beta = 90$. The normalized values of $\sigma_F/\sigma_c$ for the cubic concrete specimens having these 6 scenarios are given in Figure 12. The normalized values were used for equalization.

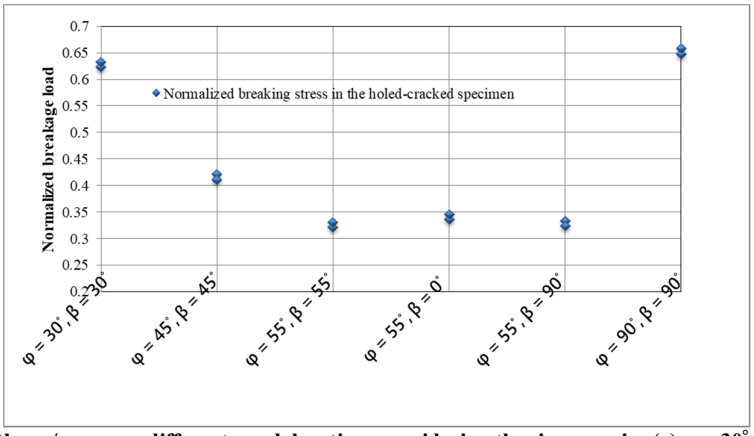


**Figure 12. Comparing the $\sigma_F/\sigma_c$ versus different crack locations considering the six scenarios (a) $\varphi = 30^\circ$, $\beta = 30^\circ$, (b) $\varphi = 45^\circ$, $\beta = 45^\circ$, (c) $\varphi = 55^\circ$, $\beta=55°$, (d) $\varphi = 55^\circ$, $\beta = 0^\circ$, (e) $\varphi = 55^\circ$, $\beta = 90^\circ$, (f) $\varphi = 90^\circ$, $\beta = 90^\circ$ for the pre-cracked cubic specimens containing two holes.**

## 5. Conclusions

The crack analysis of brittle geo-materials such as concretes and rocks under various loading conditions is important in many engineering disciplines concerning the surface and underground structures. In this research work, it was tried to investigate the complicated process of the crack growth mechanism in specially prepared cubic concrete specimens. These specimens contained two vertically arranged holes in the central part with two pre-existing cracks just above and below the upper and lower holes, respectively. Various scenarios of cracks arrangements were considered, and the specimens were numerically modelled under the different lateral confinements of 1 MPa (low), 3 MPa (medium), 6 MPa (relatively high), and 9 MPa (high). The following main conclusions may be gained from this work:

- The number of tensile cracks is decreased as the confining pressure increases. This is due to the crack closure phenomenon under the lateral confinement.
- The number of shear crack is increased by increasing the lateral confinement.
- The fracturing pattern changes from a single tensile crack to that of the several shear bands by increasing the confining pressure.
- The length of the major fracturing pattern sets is decreased by increasing the confining pressure.
- The position of fracturing is changed from the tips or near the tips of the pre-existing cracks to that of the centrally edge model starting from the center of the two cracks under the lateral confinement.
- The ultimate strength of the cubic concrete specimen is increased by increasing the confining pressure.
- The minimum strength of the specimens occurs when the crack and hole arrangements are $\varphi = 55^\circ$ and $\beta = 55^\circ$, and the maximum strength is obtained at $\varphi = 90^\circ$ and $\beta = 90^\circ$.
- The corresponding numerical results are in good agreement with their experimental counterparts.

## References

[1]. Huang, D., Gu, D. and Yang, C. (2016). Investigation on Mechanical Behaviors of Sandstone with Two Pre-existing Flaws under Triaxial Compression. Rock Mech Rock Eng. 49: 375–399.

[2]. Tian, J., Xu, D. and Liu, T. (2020). An experimental investigation of the fracturing behavior of rock-like materials containing two V-shaped parallelogram aws. International Journal of Mining Science and Technology. (06): 777-783.

[3]. Ke, C.C, Chen, C.S., and Tu, C.H. (2008). Determination of fracture toughness of anisotropic rocks by boundary element method. Rock Mech. Rock. Engin. 41: 509–538.

[4]. Yang, S.Q. (2011). Crack coalescence behavior of brittle sandstone samples containing two coplanar assures in the process of deformation failure. Engineering Fracture Mechanics. 78 (17): 3059-3081.

[5]. Shen, W., Yan, R.J., Barltrop, N., and Song, M. (2016). Fatigue crack growth analysis of T junction under biaxial compressive-compressive loading. Engineering Fracture Mechanics. 154: 207–224.

[6]. Bobet, A. and Einstein, H.H. (1998a). Fracture coalescence in rock-type materials under uniaxial and biaxial compressions. Int. J. Rock Mech Min, Sci. 35:863–888.

[7]. Bobet, A. and Einstein, H.H. (1998b). Numerical modeling of fracture coalescence in a model rock material. Int. J. Fracture 92:221–252.

[8]. Pu, C.Z. and Cao, P. (2012). Failure characteristics and its influencing factors of rock-like material with multi-fissures under uniaxial compression. Transactions of Non-ferrous Metals Society of China. 22 (1): 185-191.

[9]. Wong, L.N.Y. and Einstein, H.H. (2009). Systematic evaluation of cracking behavior in specimens containing single aws under uniaxial compression. Int J Rock Mech Min Sci. 46 (2): 239–249.

[10]. Lee, S. and Ravichandran, G. (2003). Crack initiation in brittle solids under multi-axial compression. Engin. Fract. Mech. 70:1645–1658.

[11]. Li, Y.P., Chen, L.Z., and Wang, Y.H. (2005). Experimental research on pre-cracked marble under compression. Int. J. Solids and Structures 42: 2505–2516.

[12]. Yang, Q., Dai, Y.H., Han, L.J., and Jin, Z.Q. (2009). Experimental study on mechanical behavior of brittle marble samples containing different flaws under uniaxial compression. Engin. Fract. Mech. 76:1833-1845S.

[13]. Park, C.H. and Bobet, A. (2010). Crack initiation, propagation and coalescence from frictional flaws in uniaxial compression. Engin Fract Mech 77: 2727–2748.

[14]. Zhao, Y., Zhang, L., and Wang, W. (2016). Cracking and Stress–Strain Behavior of Rock-Like Material Containing Two Flaws under Uniaxial Compression. Rock Mech Rock Eng. 49: 2665–2687.

[15]. Yang, S.Q. (2011). Crack coalescence behavior of brittle sandstone samples containing two coplanar fissures in the process of deformation failure. Engin. Fract. Mech. 78:3059-3081.

[16]. Lee, H. and Jeon, S. (2011). An experimental and numerical study of fracture coalescence in pre-cracked specimens under uniaxial compression. Int. J. of Solids and Structures 48:979-999.

[17]. Wei, C., Li, Y., Zhu, W., Li, S., Wang, S., and Wang, H., (2020). Experimental observation and numerical investigation on propagation and coalescence process of multiple flaws in rock-like materials subjected to hydraulic pressure and far-field stress. Theoretical and Applied Fracture Mechanics, https://doi.org/10.1016/j.tafmec.2020.102603.

[18]. Reis, J.M.L. and Nunes, L.C.S. (2014). Experimental investigation of mixed-mode-I/II fracture in polymer mortars using digital image correlation method. Latin American journal of solids and structures. 11: 330–343.

[19]. Tang, C.A., Lin, P., Wong, R.H.C., and Chau, K.T. (2001). Analysis of crack coalescence in rock-like materials containing three flaws—Part II: Numerical approach. Int. J. Rock Mech. Min. Sci. 38: 925–939.

[20]. Iturrioz, I., Miguel, L.F.F, and Riera, J. D. (2009). Dynamic fracture analysis of concrete or rock plates by means of the Discrete Element Method. Latin American journal of solids and structures 6:229–245.

[21]. Marji, M.F., Hosseinin_Nasab, H, and Kohsary, A.H. (2006). On the uses of special crack tip elements in numerical rock fracture mechanics. Int. j. Solids and Structures 43: 1669-1692.

[22]. Marji, M.F., Hosseini-nasab, H., and Hossein morshedy, A. (2009). Numerical modeling of the mechanism of crack propagation in rocks under TBM disc cutters. J. Mech. Mater. Struct. 2: 439-457.

[23]. Marji, M.F. (2013). On the Use of Power Series Solution Method in the Crack Analysis of Brittle Materials by Indirect Boundary Element Method. Engin Fract Mech 98: 365–382.

[24]. Haeri, H., Shahriar, K., Marji, M.F., and Moaref Vand, P. (2014). On the HDD analysis of micro cracks initiation, propagation and coalescence in brittle substances. Arab. J. geosc. doi:10.1007/s12517-014-1290-5.

[25]. Haeri, H. (2015). Propagation Mechanism of Neighboring Cracks in Rock-like Cylindrical Specimens under Uniaxial Compression, Journal of Mining Science, No. 3.

[26]. Zhang, L. and Zhu, J. (2020). Analysis of Mechanical Strength and Failure Morphology of Prefabricated Closed Cracked Rock Mass under Uniaxial Compression. Geotech Geol Eng. 38: 4905–4915.

[27]. Hao, X.A., Yqa, B., Gang, W., Cheng, F.A., Mw, E. and Rui, W.F. (2020). Discrete element study on mesomechanical behavior of crack propagation in coal samples with two prefabricated ssures under biaxial compression. Powder Technology. 375: 42-59.

[28]. Haeri, H., Sarfarazi, V., Zhu, Z., and Nejati, H.R. (2019). Numerical simulations of fracture shear test in anisotropy rocks with bedding layers. Advances in Concrete Construction: 7 (4): 241-247.

[30] Zhao W, Huang R, and Yan M (2015) Mechanical and fracture behavior of rock mass with parallel concentrated joints with different dip angle and number based on pfc simulation. Geomechanics and Engineering. 8 (6): 757-767.

[31] Li, H. and Wong, L. (2012). Influence of flaw inclination angle and loading condition on crack initiation and propagation. International Journal of Solids and Structures. 49 (18): 2482-2499.

[32] Hazzard, J.F., Young R.P., and Maxwell S.C. (2000) Micro-mechanical modeling of cracking and failure in brittle rocks Journal of Geophysical Research. 105 (B7): 16683-16697.

[33] Park, E.S. (2004) Simulation of the mechanical behavior of discontinuous rock masses using a bonded-particle model Proceedings from gulf rocks 2004, the 6th North America rock mechanics symposium

(NARMS), American Rock Mechanics Association (ARMA) 55-60.

[34] Holt, R.M. and Kjølaas, J. (2005) Comparison between controlled laboratory experiments and discrete particle simulations of the mechanical behavior of rock International Journal of Rock Mechanics and Mining Sciences. 42 (7–8): 985-995.

[35] Yoon J. (2007) Application of experimental design and optimization to PFC model calibration in uniaxial compression simulation International Journal of Rock Mechanics and Mining Sciences. 44 (6): 871-889.

[36] Cho N. and Martin, C.D. (2007) A clumped particle model for rock International Journal of Rock Mechanics and Mining Sciences. 44 (7): 997-1010.

# مطالعه مکانیسم انتشار ترک‌های ناشی از دو حفره مجاور در نمونه‌های بتنی مکعبی تحت فشارهای جانبی مختلف

**محمد داوود یاوری[1]، هادی حائری[2*]، وهاب سرفرازی[3]، محمد فاتحی مرجی[4]، حسینعلی لازمی[1]**

۱- بخش مهندسی معدن، دانشگاه آزاد اسلامی واحد بافق، بافق، ایران
۲-آزمایشگاه اصلی دولتی برای ژئومکانیک عمیق و مهندسی زیرزمین، پکن، چین
۳- بخش مهندسی معدن، دانشگاه صنعتی همدان، همدان، ایران
۴-بخش مهندسی استخراج معدن، دانشکده معدن و متالورژی، دانشگاه یزد، یزد، ایران
ارسال ۲۰۲۱/۰۵/۱۲، پذیرش ۲۰۲۱/۰۸/۰۶
* نویسنده مسئول مکاتبات: haerihadi@gmail.com

**چکیده:**

مکانیسم انتشار ترک‌های ناشی از دو حفره در نمونه‌های بتنی با در نظر گرفتن اثرات تنش‌های فشاری جانبی مختلف مورد مطالعه قرار گرفته است. تعدادی نمونه بتنی ترکدار با دو حفره مجاور تحت آزمون فشار تک محوری در آزمایشگاه مورد بررسی قرارگرفته است. بخش مدل سازی عددی تحت هر دو فشار تک محوری و فشار جانبی توسط کد جریان ذرات دو بعدی (PFC2D) انجام شده است. نتایج نشان می‌دهد که فشار جانبی ممکن است مسیر انتشار ترک را در یک نمونه بتنی در مقایسه با نمونه‌ای که تحت فشار تک محوری قرارگرفته است، تغییر دهد. حالت‌های مختلفی از انتشار ترک شعاعی در اطراف حفره‌ها بدست می‌آید و هر دو ترک بالی (کششی) و ترک ثانویه (برشی) در مسیرهای مختلف به دلیل تغییر فشار محدود تولید و منتشر می‌شوند. الگوی شکست با افزایش فشار محدود از یک ترک کششی به چندین نوار برشی تغییر می‌کند. همچنین تعداد ترک‌های برشی با افزایش فشار جانبی افزایش می‌یابد. از طرف دیگر، با افزایش فشار جانبی، ترک‌های بالی رشد خود را از دیواره‌ها شروع کرده و در محدوده‌های بالا به مرکز ترک‌ها می‌رسند .

**کلمات کلیدی:** مدل سازی آزمایشگاهی، مسیر انتشار ترک، تنش جانبی، نمونه های ترکدار، PFC2D.